EUROPEAN ORGANIZATION FOR NUCLEAR RESEARCH

CERN-PPE/91-161
03.09.1991

Precision Measurement of Antiprotonic Hydrogen and Deuterium X-Rays

K. Heitlinger[1)*], R. Bacher[2)**], A. Badertscher[2)***], P. Blüm[1)], J. Eades[3)], J. Egger[2)], K. Elsener[3)], D. Gotta[4)], E. Morenzoni[2)] and L.M. Simons[2)]

Abstract

X-rays from antiprotonic hydrogen and deuterium have been measured at low pressures. Using the cyclotron trap, a 105 MeV/c antiproton beam from LEAR was stopped with an efficiency of 86% in 30 mbar hydrogen gas in a volume of only 100 cm^3. The X-rays were measured with Si(Li) detectors and a Xe-CH_4 drift chamber. The strong interaction shift and broadening of the Lyman α transition and the spin-averaged 2p width in antiprotonic hydrogen was measured with unprecedented accuracy. The triplet component of the ground state in antiprotonic hydrogen was determined for the first time.

(submitted to Z. Phys. A - Hadrons and Nuclei)

1) Kernforschungszentrum Karlsruhe GmbH, Institut für Kernphysik and Institut für Experimentelle Kernphysik der Universität, W-7500 Karlsruhe, Germany
2) Paul Scherrer Institut (formerly Schweizerisches Institut für Nuklearforschung), CH-5232 Villigen (PSI), Switzerland
3) CERN, CH-1211 Geneva 23, Switzerland
4) Forschungszentrum Jülich GmbH, Institut für Kernphysik, W-5170 Jülich, Germany
* present address: Universität Tübingen, Auf der Morgenstelle 14, W-7400 Tübingen, Germany
** present address: DESY, Notkestr. 85, W-2000 Hamburg 52, Germany
*** present address: Institute of Intermediate Energy Physics, ETH Zürich, CH-5232 Villigen PSI

1. Introduction

Light antiprotonic atoms provide an important testing ground for models of the strong interaction at low energies. The energy levels of these exotic atoms, whose wave functions overlap the wave function of the nucleus, are shifted and broadened by the hadronic nucleus-antiproton interaction. The spectrum of these states therefore measures the strong interaction parameters at threshold. In particular, the elementary $p\bar{p}$ system (protonium or antiprotonic hydrogen) is a test case for theoretical models of low energy $N\bar{N}$ forces: indeed, the hadronic shift ε_{1s} and the broadening Γ_{1s} of the atomic ground state are related to the S-wave scattering length. The present knowledge of antiprotonic hydrogen and deuterium largely stems from experiments performed since the advent of LEAR at CERN. Recent reviews describe in detail the experimental and theoretical situation [1-3].

The measurement of ε_{1s} and Γ_{1s} is most favourable through the observation of the Kα ($2p\rightarrow 1s$) transition. However, the measurement of X-rays from antiprotonic hydrogen is complicated by several effects:

- The yield of the Kα transition is found to be only $\approx$1% of the 2p level population even at low pressures due to the strong absorption from p states. A large background originating from primary and secondary annihilation products obscures the X-ray spectrum.

- Most of the cascade processes and therefore the X-ray yields in protonium are strongly pressure dependent [4-6]. Therefore the yields increase rapidly with decreasing density, i.e. a high population of the 2p state demands the formation of antiprotonic hydrogen at low gas pressure.

In order to achieve high stop densities at very low gas pressure, where the yields of Balmer and therefore also the subsequent Lyman X-rays are expected to be maximised, a novel instrument has been built: the cyclotron trap [7,8]. This device was successfully used in first experiments on antiprotonic hydrogen and helium isotopes using 309 and 202 MeV/c beams from LEAR (experiment PS175, ref. [9,10]). Detailed account of the measurement technique and the results obtained so far in hydrogen and deuterium is given in a recent paper [9].

In the present work, a substantially improved measurement with essentially the same equipment as was used in [9] is reported. As expected, the lower beam momentum of 105 MeV/c from LEAR leads to an improved injection into the cyclotron trap, resulting in a substantially higher stop efficiency and a much improved peak to background ratio in the X-ray spectra. We can report a precision measurement of the strong interaction shift and broadening of the ground state and of the hadronic width of the 2p level in protonium. The quality of the data allows the first determination of the strong interaction shift and broadening of the triplet component of the ground state of protonium.

2. Experiment

2.1. Cyclotron trap

In the present experiment a major improvement was the fact that a 105 MeV/c antiproton beam could be used with high intensity (about 10^5 $\bar{p}$/s), good stability, and an excellent focus (about 1 mm^2). Thus a very high stop efficiency at low pressures in a small volume could be achieved in the cyclotron trap (Fig. 1a). The low beam momentum requires a special beam-tube appendix to reduce the effects of range and angular straggling (Fig. 1b). After injection into the field of the superconducting split-coil magnet, the particles are degraded from the beam momentum to the momentum accepted by the trap. As the antiprotons perform betatron oscillations around equilibrium orbits, their kinetic energy is decreased slowly by the energy loss in the target gas. The weak focussing magnetic field guides the particles to the center of the magnet, where they stop in a volume of roughly 100 cm^3. The stop efficiency of the cyclotron trap is calculated by counting the primary and secondary annihilation products in thin plastic scintillators (annihilation counters) placed between the target chamber and the cryostat walls. Annihilations in the gas are discriminated from annihilations in the beam tube and the degrader by the longer antiproton flight time between the thin scintillator at the entrance window of the target chamber and the annihilation counters. Fig. 2 shows the time distribution of annihilations at 30 mbar hydrogen gas pressure. Only a small fraction of the beam annihilates at the time of injection or during the first few turns of deceleration while 86% of the incoming antiprotons are stopped in the gas. The width of the gas peak is given by momentum straggling. The stop efficiency as a function of gas pressure and beam momentum is shown in Fig. 3. When compared to [9], the improvement in the present experiment using the lower beam momentum is clearly visible. A pressure of 30 mbar was chosen for the high statitistics

measurement of the Lyman X-rays as a compromise between stop efficiency and population of the 2p level (see below).

The geometrical size of the stop distribution, i.e. the size of the X-ray source, was determined in a series of measurements with nitrogen gas at equivalent target pressure (7.3 mbar). X-rays from $\bar{p}N$ were measured with a Si(Li) detector mounted at one bore hole of the magnet. The radial stop distribution was obtained by inserting collimators with holes of different diameters between the stop distribution and this detector. To measure the axial stop distribution a movable plastic cylinder (diameter 40 mm) was inserted into the target gas. In this way, only the antiprotons decelerating and stopping outside the obscured range could annihilate in the gas. These produce antiprotonic nitrogen X-rays, with which the stop distribution could be mapped. The plastic cylinder, however, disturbs the adiabatic deceleration in the gas so that only an upper limit for the size of the axial stop distribution can be inferred (about ±40 mm). On the other hand, since it is the X-rays and not the antiprotons which are stopped in the collimators, a radial size of the stop distribution of 60 mm diameter can be extracted with confidence from the data.

Commercially available H_2 (99.9997 %) and D_2 (99.4 %) was used. The gas pressure was monitored and stabilized by passing a constant flow through a needle valve into the target chamber and pumping at the opposite side. In this way, contamination from outgassing could be minimized, and only weak antiprotonic oxygen contaminations from water vapor are in the X-ray spectra (see below). In addition, the target gas was changed from hydrogen to deuterium at least once every 10 hours, in order to obtain information on such background X-ray lines under identical measuring conditions. Moreover, the comparison of the $\bar{p}H$ with the $\bar{p}D$ spectra served as a check for the K transitions in $\bar{p}H$: at the present level of accuracy, no K transitions in $\bar{p}D$ are expected to be observed.

2.2. Silicon X-ray detectors

X-rays were detected in this experiment by two Si(Li) detectors inserted in an axial borehole of the cyclotron trap. The first one (in the following called Si(Li)-1) of 6 mm thickness was mounted in a guard ring configuration: the signals from the outer ring detector of 200 mm^2 were used to suppress events from (spatially extended) electromagnetic showers induced by the annihilation products, whereas the inner detector (approximately 30 mm^2) was used to record X-rays (for further details see [9,11,12]). The in-beam resolution of the inner detector was measured to be 280 eV at 6.4 keV. For the measurement of the absolute yields of the L-series, this detector was placed axially at z=154 mm, in order to avoid uncertainties in the solid angle. From in-beam measurements with calibrated sources, the efficiency of the detector was found to be independent of beam intensity variations. For the high statistics K X-ray experiment, however, it was placed much closer to the stop distribution (z=64 mm), in order to increase the solid angle. In addition, it was found that the peak to background ratio was favorable at a closer distance: showers from annihilation products cause more background in the bore hole region around z=150 mm, where the magnetic field of the cyclotron trap tends to focus the shower electrons. Finally, this close position allowed a high statistics measurement of the L Xrays. Relative yields of the different L and K lines could be measured with high accuracy in the same detector and lead to a new determination of the 2p width as well as a precise check of the cascade parameters (see below).

The second detector (Si(Li)-2), a conventional large area Si(Li) of 300 mm^2 sensitive area and a thickness of 5 mm, was placed at a distance of z=69 mm in the opposite bore hole. The in-beam resolution was measured to be 590 eV at 6.4 keV. It was only used for the high statistics measurement of the Kα transition.

2.3. X-ray drift chamber

The X-ray drift chamber had a 16 x 16 cm^2 sensitive area and was filled with a 90% Xe and 10% CH_4 gas mixture. It was mounted radially to the target chamber, opposite to the antiproton injection point at a distance of 100 cm from the center of the magnet (Fig. 1b). X-rays are converted to electrons by photoeffect in the 4 cm absorption gap. The swarm of charges produced by stopping these electrons is drifted to the proportional gap, where it is amplified. Pulse height, pulse width and drift time of the 16 anode wires and 16 cathode strips were recorded. The in-beam energy resolution of the drift chamber was measured to be 11% (FWHM) at 9 keV.

In the drift chamber, most of the "good" photons (X-rays) are absorbed in the drift region. The photo-electrons produced have a short range of about 1 mm. A "good" event is defined as a short anode signal of 150 to 200 ns, corresponding to a drift path difference up to 2 to 3 mm. The drift time interval is restricted to 0.2 to 2.2 µs after an antiproton stop to suppress events not originating from the gas peak (see Fig. 2). The rejected prompt events (< 200 ns) are mainly minimum ionizing particles traversing the detector. These electrons are components of showers generated by the numerous pions created in the $\bar{p}$ annihilation, and are accompanied by Bremsstrahlung photons responsible for the background in the X-ray spectrum. The granularity of the drift chamber (a cell of 1cm x 1cm from the 16 anodes and cathodes, and

0.4 cm pulse-to-pulse separation in the drift direction) allows the rejection of a large amount of these many-photon shower events.

Therefore, the first step in analyzing the data from the drift chamber was filtering: only events with one single anode and one single cathode pulse above a threshold of 0.2 keV and 0.5 keV, respectively, were accepted. In addition, the duration of these pulses was required to be inside an interval corresponding to a drift path difference of a few mm. Furthermore, no events from the cells next to the chamber walls were accepted.

The second step is a fit to the two-dimensional (energy vs. drift length) distribution of the events. The distribution of drift lengths shows an exponential behaviour as expected, and exhibits the correct energy dependent absorption length. This is true for the "good" X-rays from antiprotonic atoms, but also for Bremsstrahlung single photons which are responsible for a part of the background in the X-ray spectra (see Fig. 10). In addition, we consider two other sources of background in the fit of the data: (1) When high energy γ-rays simulate an X-ray due to Compton effect in the gas, they produce a background with a flat distribution in the drift length over the full depth of 20 mg/cm^2 of the detector. (2) Conversion of photons and Compton scattering of γ-rays at the inner surface of the drift chamber window are responsible for background events located in the first few millimeters of the drift region in the gas.

All three types of background were assumed to be given by Gaussian line shapes with exponential tails. Identical shape parameters are used for p̄H, p̄D and the calibration spectra (p̄N, p̄O, p̄C, p̄Ne). With the latter, energy, energy dependent absorption behavior of X-ray lines and the solid angle and efficiency of the drift chamber could be calibrated.

2.4. Calibration of the detectors

The detector calibration with respect to energy, resolution and relative efficiency was performed with the method of completely ionized antiprotonic atoms [13]. Within a few percent, the radiative transitions have equal yields, allowing the relative efficiency calibration of the Si(Li) detectors and the X-ray drift chamber down to the lowest detectable energies. Typical calibration spectra are shown in Fig. 4a for the detector Si(Li)-1, in Fig. 4b for the drift chamber. The measured efficiency curve of the detector Si(Li)-1 is shown in Fig. 5. The energies of the transitions were obtained from the code PBAR [14]. The absolute efficiency calibration was obtained by an in-beam measurement with a calibrated standard ^{57}Co source.

3. Results and Discussion

3.1. Balmer transitions

In order to improve the understanding of the atomic cascade in antiprotonic hydrogen and deuterium, a series of measurements was performed at gas pressures of 16, 30, 60, and 120 mbar H_2 and D_2. A selection of spectra is shown in Fig. 6. The peaks were fitted with the program FITOS [15] using Gaussian profiles. The absolute yields obtained are given in Table 1, and (for hydrogen) compared to cascade calculations in Fig. 7 (the data points are from this work and from [9]). The free parameters of the cascade code of Borie and Leon [6] were obtained from a fit to the Lα yields to be $k_{Stk} = 1.94 \pm 0.13$ and $T_{kin} = (1.0 \pm 0.2)$ eV which is consistent with the values given in [9] for hydrogen. The same set of parameters yields excellent agreement for the Lβ transition, the sum of the Balmer transitions as well as for the cascade of deuterium. This is in contrast to the results reported in [9], where smaller yields for the deuterium cascade were reported. We have now established that this was a spurious effect due to a normalization error in the deuterium run of [9]. Therefore, we now find agreement with an earlier experiment [16,17,18] and recent cascade calculations by Reifenröther and Klempt [19, 20]. A particular strong width of the 3d state is no longer needed to fit the cascade data in antiprotonic deuterium. In the limit of vanishing gas pressure, the total yield of the Balmer series is predicted to be about 98% with a small contribution of only 2% from transitions nd→2p with n≥4 [21]. This again shows the importance of collisional processes at pressures even below 16 mbar.

For a precision measurement of the 2p width via the intensity balance of the total Balmer series and the Lyman-α transition, a high statistics run was performed with the detector Si(Li)-1 at 30 mbar. Fig. 8a shows the spectra for antiprotonic hydrogen and deuterium, covering a large energy range from 1 to 18 keV. In this way, the L- and K-transitions for p̄H were measured with the same detector, avoiding difficult cross-calibrations. The hadronic 2p width was obtained from

$$\Gamma_{2p}^{abs} = \Gamma_{2p}^{rad} \left[\left(\frac{I(3\to2)}{I(2\to1)} \frac{\varepsilon^{Det}{}_{2\to1}}{\varepsilon^{Det}{}_{3\to2}} + \frac{I(4\to2)}{I(2\to1)} \frac{\varepsilon^{Det}{}_{2\to1}}{\varepsilon^{Det}{}_{4\to2}} + \ldots \right) - 1 \right] . \qquad (1)$$

The detector efficiencies ε at the various energies were obtained from calibration runs with antiprotonic nitrogen and oxygen. The radiative width of the 2p level is 0.38 meV for antiprotonic hydrogen.

In an expanded view (Fig. 8b), the Balmer X-rays are shown in more detail. Note that in addition to the electronic "reset"-peak from the preamplifier, the electronic Kα transition from the excitation of Si atoms is found in the spectrum of antiprotonic deuterium. This is taken into account in the fit of the hydrogen spectrum. From this high statistics measurement, the ratios between different Balmer transitions have been obtained very accurately - thus providing a sensitive test of the cascade calculations (Table 2). It is seen that agreement is rather good up to the Lγ transitions, whereas all the ratios including the Balmer δ transition show deviations of up to a factor 5 from the calculated ratios for both hydrogen and deuterium. This indicates that the population of the 6d state is actually larger than predicted by the cascade model, which in turn might be evidence of an increased Coulomb-deexcitation rate around n=7. (Note that similar effects have been found in pionic hydrogen [22]).

3.2. Lyman transitions

In Fig. 8c, an expanded view of the energy region of the K transitions is shown. While for hydrogen a distinct peak shows the Kα transition, no structure is seen in the antiprotonic deuterium spectrum. The fit to the spectra improves considerably when contamination lines from antiprotonic oxygen are included. As there are no nitrogen lines in the spectrum, this oxygen is assumed to stem from water vapour in the target chamber - note that the measured intensities correspond to less than 10^{-2} mbar H_2O at 30 mbar H_2. The smooth background in the deuterium spectrum can be described by a third order polynomial. The same procedure was applied to the hydrogen spectrum. The intensity and position of the antiprotonic oxygen lines were fixed in the fit. The Lyman series was fitted with a) the Kα component and b) the K_∞ component containing all (unresolved) transitions np→1s for n≥10. Using the parameters given in section 3.1, a cascade calculations shows that the total intensity of all Lyman transitions with 3≤n<10 amounts to only 6% of the intensity of the whole K series and can therefore be neglected [3,9]. The line shape was fitted with a Voigt profile, i.e. the folding of the Lorentzian due to the natural line shape and the Gaussian given by the detector resolution. No conditions were enforced on the parameters of the Voigt profiles for the Lyman transitions. The results of this analysis of the spectrum shown in Fig. 8c are given in Table 3.

Also shown in Table 3 are the results obtained from the measurement with Si(Li)-2 (Fig. 9). Note that this large area detector contains, in addition to the p̄O contamination lines, also a small contribution which is attributed to the pionic Al (5→4) transition at 14.07 keV, coming from the walls of the target chamber on the side opposite to the detector. The intensity of this line is too small to be seen in the much smaller Si(Li)-1 detector.

The spectra from p̄H and p̄D obtained with the drift chamber are shown in Fig. 10 after subtraction of the fitted non exponential background. In order to take the small water vapor contamination into account (see above), the p̄O lines with fixed energies and relative intensities are included in the fit. The shift, width and yield for p̄H were determined (Table 3). The yield ratio of Kα to K_∞ was determined to be 5.7 ± 1.8, which corresponds to a K_∞ yield of $(1.2 \pm 0.4)\cdot 10^{-3}$ if for the Kα yield the weighted average of Table 3 is used.

It should be noted that in the spectrum of antiprotonic deuterium no structures could be found which might be attributed to the Lyman transitions in this system. Predictions for the shift and broadening of the 1s state in antiprotonic deuterium [23,24,25] differ widely and therefore do not allow a specific search of the 2p→1s transition.

3.3. Triplet component of the protonium ground state

Theoretical models predict the strong interaction hyperfine splitting of the 1s state in antiprotonic hydrogen to be of the order of 300 eV. The intensity ratio should be about 2.2 : 1 according to the 2p widths given in [28], differing from the statistical 3 : 1 ratio due to the different absorption from the hyperfine levels. In view of the good energy resolution of the detector Si(Li)-1 (301 eV at 8.7 keV), and the peak to background ratio (0.17), an attempt was made to test this hypothesis. Two lines with the fixed peak ratio 2.2 were introduced in the fit to describe the Kα line shape. As the width of the two lines was left free in the fit, this condition is a rather weak one. The parameters of the contamination lines from p̄O were kept fixed, too. No other conditions were applied. The result of this fit is shown as a dashed line in Fig. 8c.

In order to test the reliability of this procedure, Monte Carlo generated spectra were analyzed: On a background corresponding to the measured one, the doublet structure of the Lyman transition was generated together with the sum of the Lyman transitions from high n states at the corresponding energy. The

triplet and singlet states were simulated with a Voigt profile containing the measured detector resolution and the assumed Lorentz width was 750 eV. The intensity ratio was again fixed to be 2.2. In a series of simulated spectra, the triplet/singlet splitting was varied in steps of 100 eV, from 100 to 700 eV. All these spectra were then analyzed with the procedure used for the measured one. (As the influence of the contamination lines was found to be small in the analysis of the data, these were not included in the Monte Carlo simulation). The result shows that position and width of the triplet component is correctly reproduced for all Monte Carlo spectra. However, the position of the singlet state is only reproducible for splittings of more than 500 eV to the triplet. Therefore, we conclude that we can reliably deduce the triplet state from our spectra, but only give an upper limit of 500 eV for the energy splitting of the two substates. Also the fit is not sensitive to the width of the singlet component (Table 3).

3.4. Comparison with strong interaction models

The present experimental result on the strong interaction shifts and widths in antiprotonic hydrogen is compared to other recent experiments and different theoretical models in Fig. 11. For the comparison the weighted average of the spin-averaged shift and widths of experiments PS174 and PS175 has been calculated and indicated in Fig. 11. Neither the results of PS171 (they were obtained with a trigger on neutral final states thus favouring the singlet state $^1S_0$) nor the result on the triplet state from the analysis of this experiment are included in this average. These new average experimental values are ε_{1s} = (-730±20) eV, Γ_{1s} = (1122±57) eV and Γ_{2p} = (34.0±2.9) meV.

In order to be consistent with the experimental results, the spin averaged 1s shift and width and the 2p width obtained fromt theoretical models have been calculated taking into account the absorption from the different 2p hyperfine levels (Fig. 11). Changing the width of these levels changes the statistical population of the 1s components and therefore the average value. The intensity ratio of triplet to singlet ground state is given by

$$\frac{Y(^3S_1)}{Y(^1S_0)} = \frac{\sum_{FF'(^3S_1)} g_{FF'} \frac{\Gamma_X}{\Gamma_X + \Gamma_F}}{\sum_{FF'(^1S_0)} g_{FF'} \frac{\Gamma_X}{\Gamma_X + \Gamma_F}} \qquad (2)$$

where $g_{FF'}$ is the statistical weight of the hyperfine transitions F→F' leading to the final states $^3S_1$ and $^1S_0$, respectively. Γ_X is the radiative 2p width and Γ_F are the hadronic 2p widths. In most cases the ratio is ≈2.5 . A statistical population of the 2p hyperfine levels can be assumed because the radiative widths are much larger than the hadronic widths for the d-states in antiprotonic hydrogen [29].

Within a 3σ confidence level most of the calculations agree with the measured spin-averaged shift and width. A consistent picture, however, using 1s shift and broadening and the 2p width, can not be obtained from any of the various models. Certainly, the spin-averaged width and the width of the triplet state require a rather large width of the singlet state, but the unknown strength of the 2p→1s hyperfine transitions as well as the unknown 1s splitting do not permit a clear statement. Only an independent determination of the shifts and widths of the ground state components can unambigously clarify the situation.

Although of a high accuracy, the spin averaged 2p strong interaction width (see Table 3) is not decisive to the calculations. Once again, the importance of the very large p-wave annihilation is clearly established in this experiment. To compare with the experimental results (Fig. 11) the spin-averaged 2p width Γ_{2p} is calculated from the predictions of the hyperfine levels:

$$\Gamma_{2p} = \frac{\sum_F (2F+1)}{\sum_F \frac{2F+1}{\Gamma_X + \Gamma_F}} \cdot \Gamma_X \ . \qquad (3)$$

This accounts for the corrections of the intensity balance relation used to determine the 2p widths. The corrections decrease the width by about 10% as compared to a statistical contribution of the 2p→1s hyperfine components.

4. Summary and Outlook

It has been shown, that the 105 MeV/c antiproton beam from LEAR can be stopped in a small volume at low gas pressure using the unique features of the cyclotron trap. With high resolution Si(Li) detectors, a high statistics measurement of X-rays from antiprotonic hydrogen was performed. The pressure dependence of the Balmer series was studied in detail for hydrogen and deuterium between 16 and 120 mbar and found to be equal within the experimental errors. Agreement was found with cascade calculations, except for the $\Delta n>2$ transitions. Precise results on the spin averaged shift and broadening of the protonium ground state were obtained as well as the strong width of the 2p state.

An independent measurement of the Kα yield was performed using a drift chamber with a good peak-to-background ratio and a large solid angle. This permitted us to deduce the 2p width from intensity balance with the Balmer transitions measured in the Si(Li)-1 detector.

The accuracy of the spin averaged values is still not selective enough when compared to theoretical calculations. Therefore, a sensitive test of the theoretical approaches requires an accurate measurement of shift and width of the different spin components. One step in this direction has been performed in the present work: for the first time, the triplet component of the $\bar{p}p$ ground state was measured directly. More work should follow, e.g. for the p-wave interaction: the predicted values for the 2p hyperfine states are very sensitive to details of the theoretical models.

Precision spectroscopy of the hyperfine components requires a step beyond the limits reached by the detection methods described here. For example, the use of charge coupled devices (CCD's) is proposed for the separation of the hyperfine ground state components in $\bar{p}$H. CCD's might even make the detection of the $\bar{p}$D Kα transition possible. With a crystal spectrometer, on the other hand, the shifts of the 2p levels can be measured and the 2p widths can be determined directly [36].

Acknowledgments

The authors would like to thank the LEAR staff for their efforts in providing the antiproton beam. The help of P. Gauss from the CERN cryogenic group and of P. Zettwoch from the PS workshop is gratefully acknowledged. We wish to thank K.-P. Wieder for his help with the drawings.This work is part of the Ph.D. thesis of one of us (K.H., University of Karlsruhe, 1990).

References

1. Batty, C.J.: Rep. Prog. Phys. **52**, 1165 (1989)
2. Batty, C.J.: Nucl. Phys. **A508**, 89c (1990)
3. Simons, L.M.: Proceedings of the Fourth LEAR Workshop Villars-sur-Ollon, Amsler, C., Backenstoss, G., Klapisch, R., Leluc, C., Tauscher, L. (eds.), Vol. 14, p. 703. London, Chur, Paris: Harwood 1988
4. Day, T.B., Snow, G.A., Sucher, J.: Phys. Rev. Lett. **3**, 61 (1959)
5. Leon, M., Bethe, H.A.: Phys. Rev. **127**, 636 (1962)
6. Borie, E., Leon, M.: Phys. Rev. **A21**, 1460 (1980)
7. Simons, L.M.: Phys. Scrip. **T22**, 90 (1988)
8. Simons, L.M., Bacher, R., Blüm, P., Gotta, D., Kunold, W., Schneider M.: to be published
9. Bacher, R., Blüm, P., Gotta, D., Heitlinger, K., Rohmann, D., Schneider, M., Egger, J., Simons, L.M., Elsener, K.: Z. Phys. A - Atomic Nuclei **334**, 93 (1989)
10. Schneider, M., Bacher, R., Blüm, P., Gotta, D., Heitlinger, K., Kunold, W., Rohmann, D., Egger, J., Simons, L.M., Elsener, K.: Z. Phys. A - Atomic Nuclei **338**, 217 (1991)
11. Schneider, M., thesis, University of Karlsruhe 1987, KfK report no. 4222 (1987)
12. Heitlinger, K., thesis, University of Karlsruhe 1990.
13. Bacher, R., Blüm, P., Gotta, D., Heitlinger, K., Missimer, J., Simons, L.M., Elsener, K.: Phys. Rev. **A38**, 4395 (1988)
14. Borie, E., and Jödicke, B., Comput. Phys. vol 2, no. 6, 61 (1988).
15. Köhler, T., Rohmann, D.: program FITOS, Cern, Geneva (1984)
16. Baker, C.A., Batty, C.J., Clark, S.A., Moir, J., Sakamoto, S., Davies, J.D., Lowe, J., Nelson, J.M., Pyle, G.J., Selvarajah, A., Squier, G.T.A., Welsh, R.E., Winter, R.G., Lingeman, E.W.A.: Nucl. Phys. **A483**, 631 (1988)

17. Van Eijk, C.W.E., Hollander, R.W., Langerveld, D., Okx, W.J.C., Zoutendijk, A., Feirreira-Marques, R., Baker, C.A., Batty, C.J., Clark, S.A., Moir, J., Sakamoto, S., Davies, J.D., Lowe, J., Nelson, J.M., Pyle, G.J., Squier, G.T.A., Welsh, R.E., Winter, R.G., Lingeman, E.W.A.: Nucl Phys. **A486**, 604 (1988)
18. Baker, C.A., Batty, C.J., Moir, J., Sakamoto, S., Davies, J.D., Lowe, J., Nelson, J.M., Pyle, G.J., Squier, G.T.A., Welsh, R.E., Winter, R.G., Lingeman, E.W.A.: Nucl. Phys. **A494**, 507 (1989)
19. Reifenröther, G., Klempt, E.: Nucl Phys. **A503**, 885 (1989)
20. Reifenröther, G., Klempt, E.: Phys. Lett. **B245**, 129 (1990)
21. Cohen, J.S., Padial, N.T.: Phys. Rev. **A41**, 3460 (1990)
22. A.J. Rousi-El-Hassani, PhD thesis ETH Zürich No. 9256 (1990)
23. Wycech, S., Green, A.M., Niskanen, J.A.: Phys. Lett. **B152**, 308 (1985)
24. Latta, G.P., Tandy, P.C.: Phys. Rev. **C42**, R1207 (1990)
25. Liu, G.Q., Richard, J.M., Wycech, S.: Phys. Lett. **B260**, 15 (1991)
26. Barmo, S., Pilkuhn, H., Schlaile, H.G.: Z.Phys. A - Atomic Nuclei **A301**, 283 (1981)
27. Ziegler, M., Ahmad, S., Amsler, C., Armenteros, R., Auld, E.G., Axen, D., Bailey, D., Barlag, S., Beer, G., Bizot, J.C., Botlo, M., Comyn, M., Dahme, W., Delcourt, B., Doser, M., Duch, K.D., Erdmann, K., Feld-Dahme, F., Gastaldi, U., Heel, M., Howard, B., Howard, R., Jeanjean, J., Kalinowsky, H., Kayser, F., Klempt, E., Laa, C., Landua, R., Marshall, G., Nguyen, H., Prevot, N., Riedlberger, J., Rieger, R., Roberston, L., Sabev, C., Schaefer, U., Schreiber, O., Straumann, U., Truöl, P., Vonach, H., Weidenauer, P., White, B.L., Wodrich, W.R.: Phys. Lett. **B206**, 151 (1988).
28. Kaufmann, W.B., Pilkuhn, H.: Phys. Rev. **C17**, 251 (1978)
29. Carbonell, J., Ihle, G., Richard, J.M.: Z. Phys. A - Atomic Nuclei **334**, 329 (1989)
30. Kohno, M., Weise, W.: Nucl Phys. **A454**, 429 (1986)
31. Green, A.M., Wycech, S.: Nucl. Phys. **A377**, 441 (1982)
32. Schweiger, W., Haidenbauer, J., Plessas, W.: Phys. Rev. **C32**, 1261 (1985)
33. Moussallam, B.: Z. Phys. A - Atomic Nuclei **325**, 1 (1986)
34. Dalkarov, O.D., Protasov, K.V., Shapiro, I.S.: Int. J. Mod. Phys. **A5**, 2155 (1990)
35. Thaler, J.: J. Phys. G: Nucl. Phys. **9**, 1009 (1983).
36. Anagnostopoulos, D., Borchert, G.L., Gotta, D., Schult O.W.B.,Simons, L.M., Elsener, K., Rashid, K., Reidy, J.J., Deslattes, R., Mooney, T., Cowan, P., Indelicato, P., Bovet, E.D., Chatellard, D., Egger, J.-P., Jeannet, E.: proposal CERN/PSCC/90-9/P124 (1990)

Table 1: Measured absolute yields of the Balmer transitions in antiprotonic hydrogen and deuterium.

	pressure (mbar)	Y(Lα) (%)	Y(Lβ) (%)	$Y(L_{tot})$ (%)
$\bar{p}p$	16	53.2 ± 9.3	7.7 ± 2.4	71.9 ± 10.0
	30	40.2 ± 5.0	6.2 ± 1.3	55.1 ± 5.6
	60	31.9 ± 3.8	4.8 ± 0.9	44.3 ± 4.1
	120	26.5 ± 3.3	5.2 ± 1.0	38.9 ± 3.7
$\bar{p}d$	16	50.2 ± 5.7	9.4 ± 3.6	69.3 ± 7.3
	30	33.4 ± 3.5	5.3 ± 1.0	46.0 ± 3.9
	60	28.3 ± 2.9	3.9 ± 0.8	38.0 ± 3.2
	120	21.7 ± 2.2	2.5 ± 0.6	30.7 ± 2.5

Table 2: Comparison of measured and calculated intensity ratios of Balmer transitions in antiprotonic hydrogen and deuterium at 30 mbar. The calculated ratios are obtained with the cascade code of Borie and Leon [6] (see text). L_∞ denotes the sum of all Balmer transitions with n≥7.

	$\bar{p}p$		$\bar{p}d$	
intensity ratio	meas.	calc.	meas.	calc.
Lα/Lβ	7.1 ± 0.7	6.0	6.6 ± 0.3	6.9
Lα/Lγ	20.6 ± 2.0	27.2	19.3 ± 0.9	31.2
Lα/Lδ	23.9 ± 2.6	93.2	28.5 ± 1.6	148.2
$L\alpha/L_\infty$	6.9 ± 0.6	8.3	5.6 ± 0.2	7.9
$L\alpha/L_{tot}$	0.75 ± 0.08	0.73	0.71 ± 0.03	0.75
Lβ/Lγ	2.9 ± 0.2	4.5	2.9 ± 0.1	4.6
Lβ/Lδ	3.4 ± 0.2	15.5	4.3 ± 0.2	21.6
Lγ/Lδ	1.2 ± 0.1	3.4	1.5 ± 0.1	4.7

Table 3: Strong interaction shift and widths in antiprotonic hydrogen measured by experiment PS175. The purely electromagnetic energy of the Kα transition is 9.408 keV [26]. The spin averaged values for shift and widths of the 1s state are given. The width of the 2p level is obtained from the intensity balance between the Balmer series and the Lyman a transitions (see text). Also presented are the shift and width of the triplet component of the 1s state together with an upper limit of the energy splitting between triplet and singlet component. The first error given is purely statistical, the second one reflects the accuracy and stability of the energy calibration. For the weighted average, the two error contributions are added quadratically.

detector	Si(Li)-1 this work	Si(Li)-2 this work	driftchamber this work	Si(Li) (1986) Ref. [9]	PS175 weighted average
ε_{1s} (eV)	- 690 ± 35 ± 10	- 770 ± 30 ± 10	- 640 ± 90 ± 100	- 620 ± 100	-727 ± 23
Γ_{1s}^{abs} (eV)	1060 ± 140 ± 10	1290 ± 120 ± 10	1060 ± 260	1130 ± 170	1160 ± 78
Yield Kα (30 mbar)			(8.1 ± 1.5) 10^{-3}	(6.2 ± 1.7) 10^{-3}	(7.2 ±1.1) 10^{-3}
X^2/NDF	1.05	1.03		1.09	
peak/backgr.	0.17	0.14	0.83	0.022	
Γ_{2p}^{abs} (meV)	36 ± 4		26 ± 7	32 ± 10	33 ± 3
ε_{1s}^{T} (eV)	- 850 ± 40 ± 10				- 850 ± 41
Γ_{1s}^{T} (eV)	770 ± 150 ± 10				770 ± 150
$\Delta\varepsilon_{1s}$ (T,S) (eV)	≤ 500				≤ 500

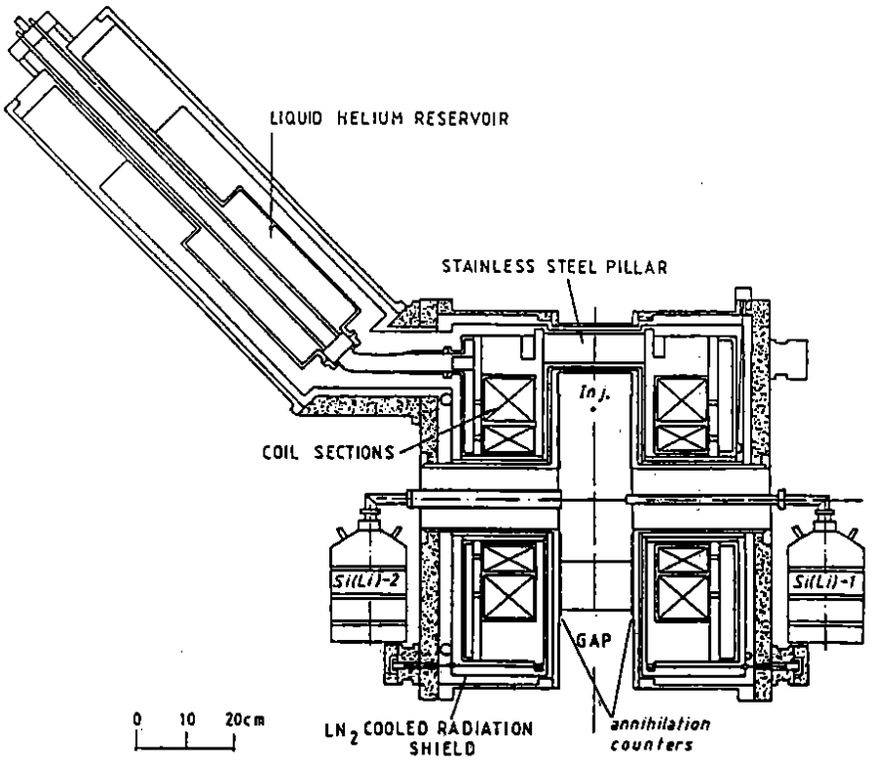

Fig. 1(a): The cyclotron trap. The z-axis is the (cylindrical) symmetry axis of the magnet. The Si(Li) detectors were mounted in the bore hole of the magnet. The scintillation counters between the target chamber and the cryostat walls detect the time of the annihilation. "Inj." denotes the injection radius of the antiproton beam perpendicular to the cross section shown.

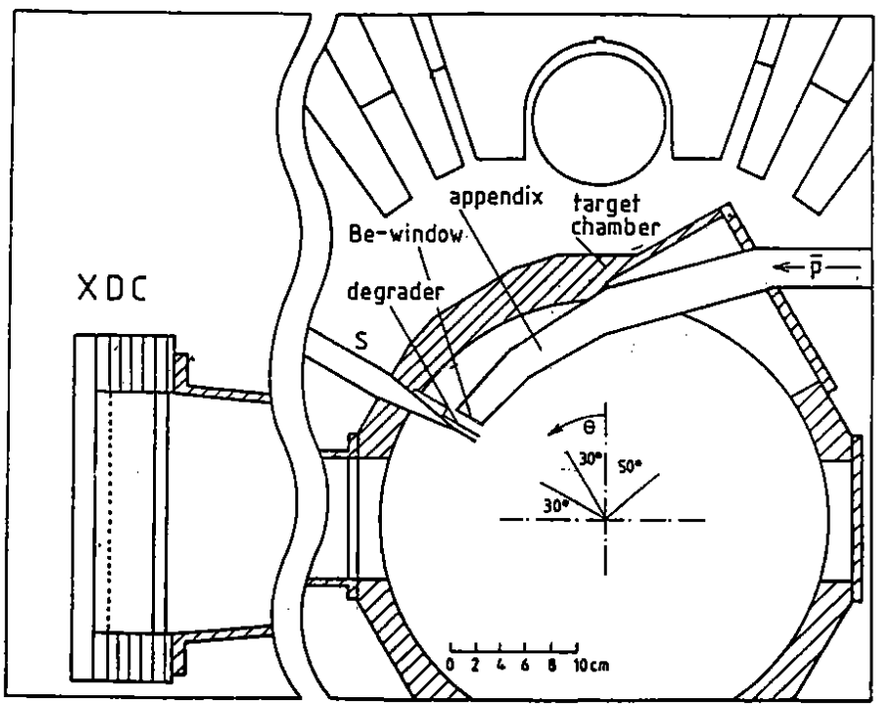

Fig.1(b): Cross section of the target chamber in the symmetry plane of the cyclotron trap. The antiproton beam enters through a curved beamline and traverses a 100 μm Be window, a mylar degrader and a plastic scintillator. The degrader thickness is optimized for each target pressure. The remaining deceleration to the capture of antiprotons takes place in the target gas. The X-ray drift chamber (XDC) was mounted at the radial opening opposite the beam injection.

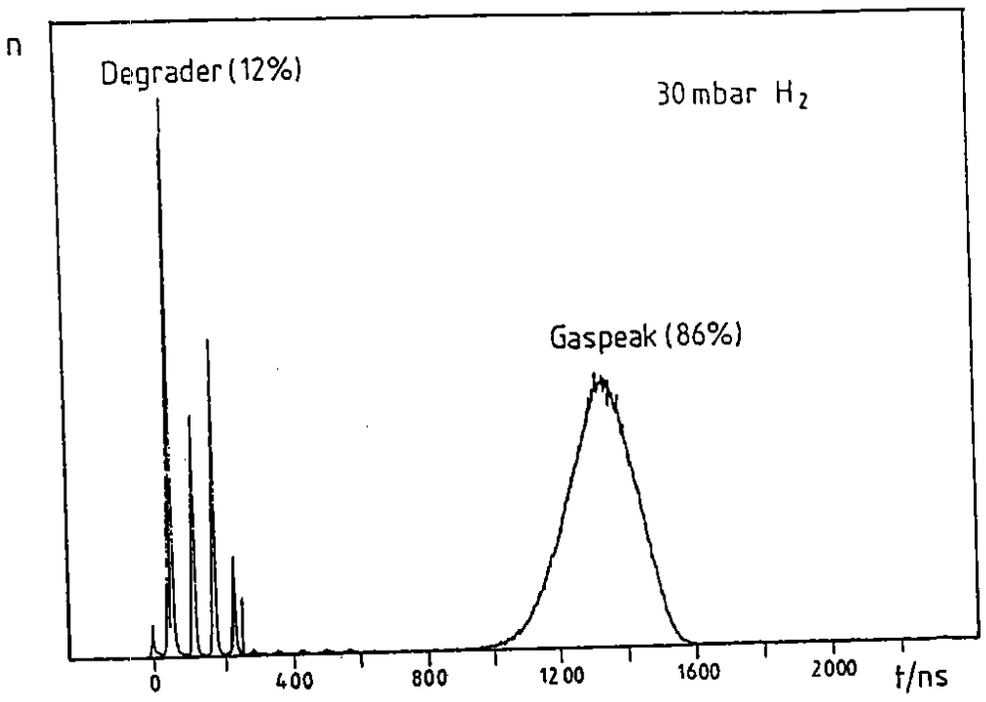

Fig. 2: Time evolution of the deceleration in the cyclotron trap at 30 mbar hydrogen: the time-of-flight spectrum shown is taken between the passage of an antiproton through the thin scintillator (denoted 'S' in Fig. 1b) at the entrance window of the target chamber ("start") and its annihilation as detected in the annihilation counters ("stop"). The broad peak at $t \approx 1250$ ns (corresponding to about 30 revolutions) is attributed to annihilations in the target gas.

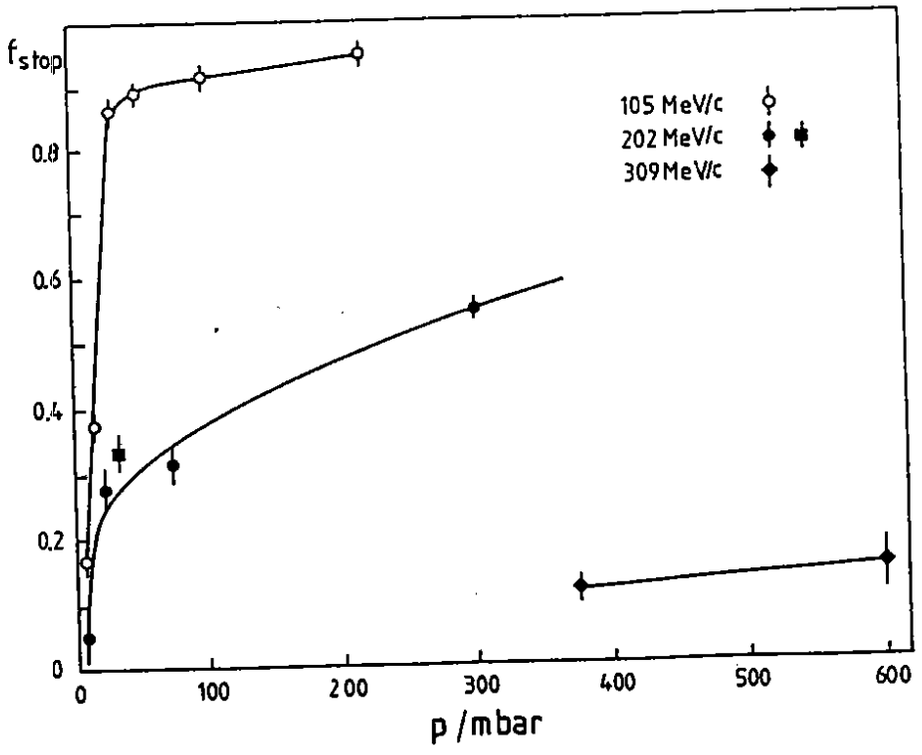

Fig. 3: Stop efficiency of the cyclotron trap as a function of hydrogen equivalent gas pressure. The data for beam momenta of 309 Mev/c [10] and 202 MeV/c [9] were obtained in earlier measurements, the upper curve in the present work using the 105 MeV/c beam from LEAR.

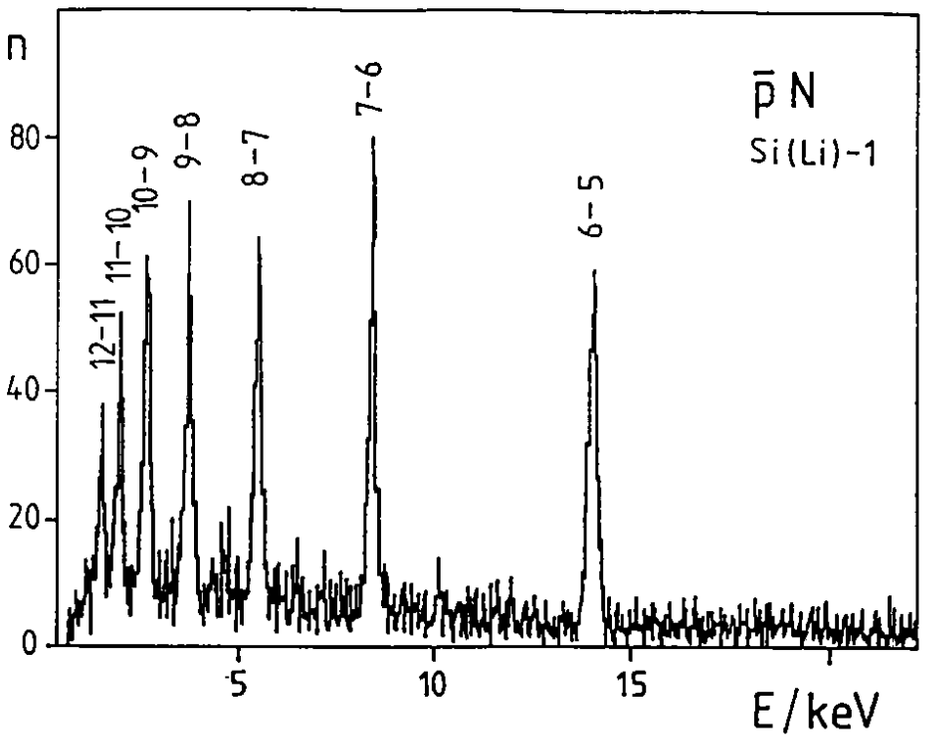

Fig. 4(a): X-ray spectrum recorded for in-beam calibration of the detector Si(Li)-1 from antiprotonic nitrogen, at a target pressure equivalent to 30 mbar hydrogen.

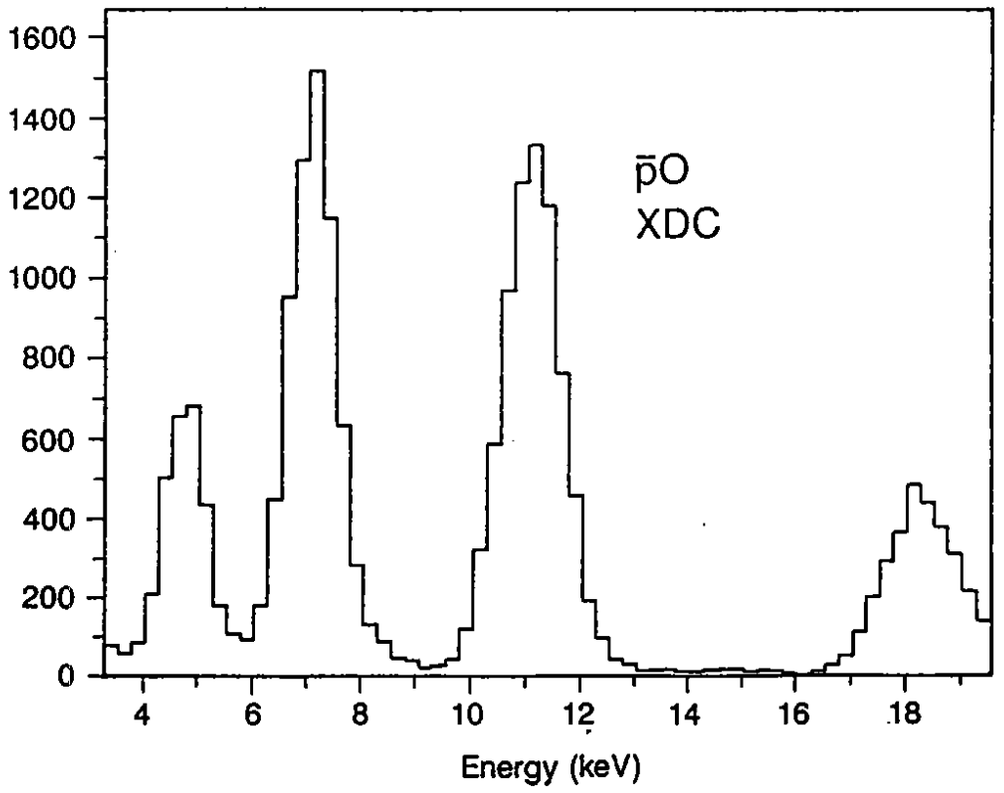

Fig. 4(b): X-ray calibration spectrum from antiprotonic oxygen measured in the X-ray drift chamber.

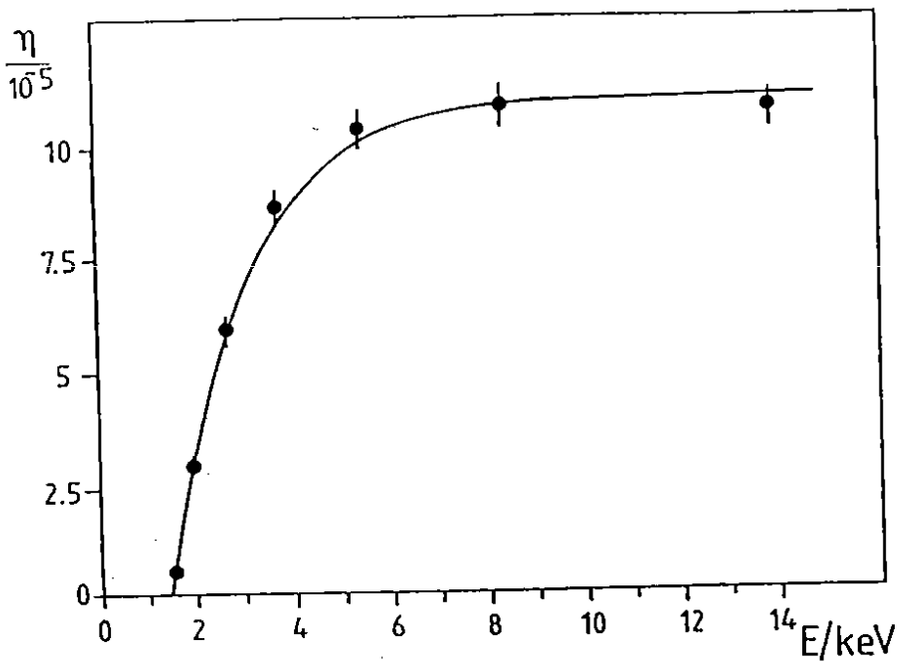

Fig. 5: Detection efficiency of the X-ray detector in guard-ring configuration (Si(Li)-1) deduced from the antiprotonic nitrogen spectra. η is the product of the intrinsic efficiency ε and the fraction of the effective solid angle $\Delta\Omega/4\pi$.

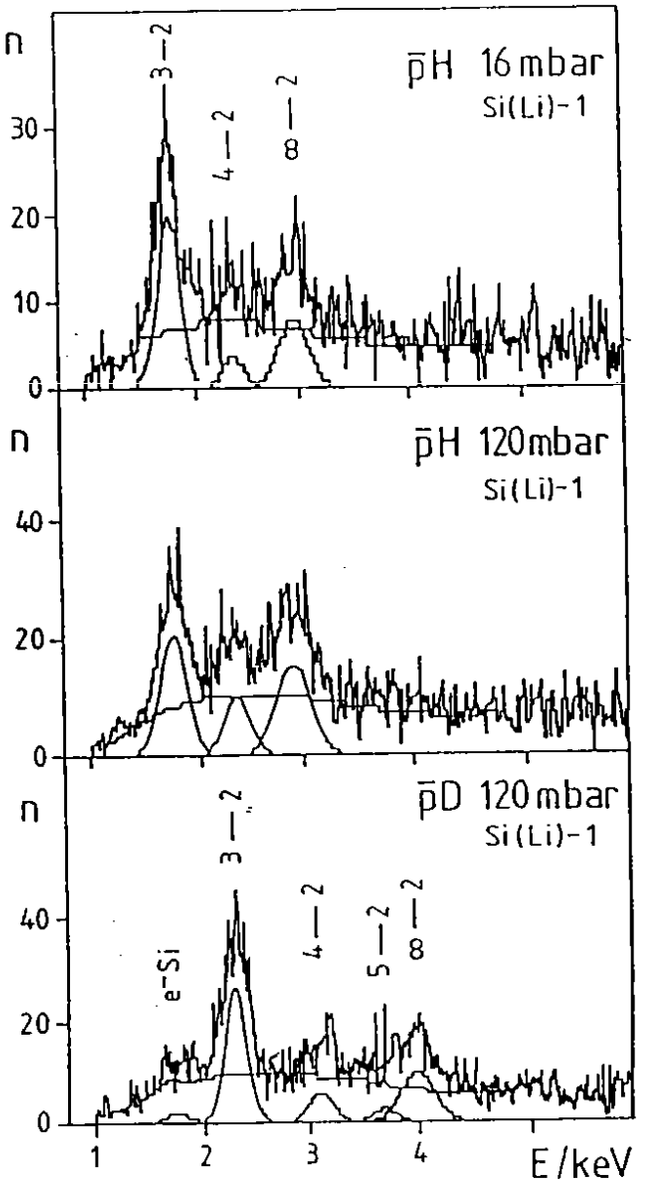

Fig. 6: Selection of spectra to study the pressure dependence of the Balmer X-ray yields measured with Si(Li)-1 at 16 mbar H_2, 120 mbar H_2 and 120 mbar D_2. Spectra are normalized to the same number of incoming antiprotons. The peak to background ratio improves substantially using the 105 MeV/c beam compared to the measurement with 202 MeV/c momentum [9].

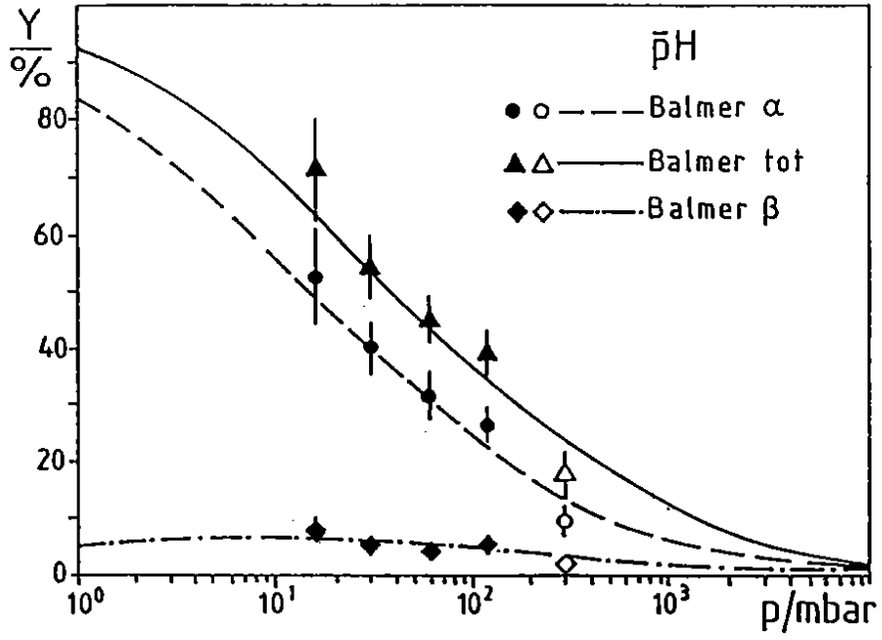

Fig. 7: Measured yields of Balmer X-rays in antiprotonic hydrogen as a function of pressure. The curves are obtained with the cascade code of Borie and Leon [6] with the parameters fitted to the measured yields (full symbols: this experiment, open symbols: ref. [9]).

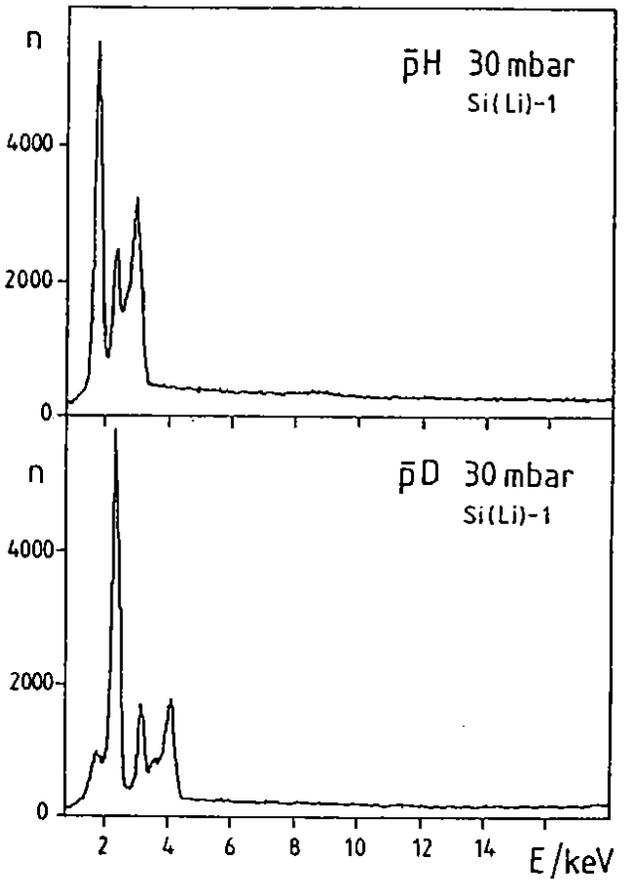

Fig. 8(a): Spectra from the high statistics run for antiprotonic hydrogen and deuterium, measured with detector Si(Li)-1 at 30 mbar. The spectrum of antiprotonic hydrogen shows both the L and K transitions.

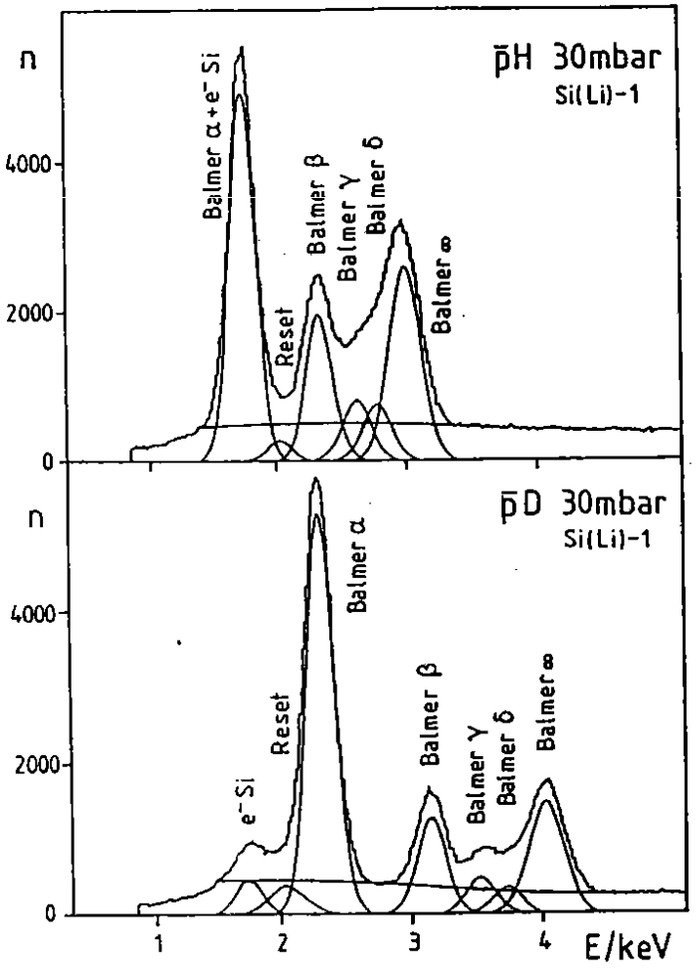

Fig. 8(b): Expanded view of the spectra shown in Fig. 8a. The low energy region comprising the Balmer series is shown in detail.

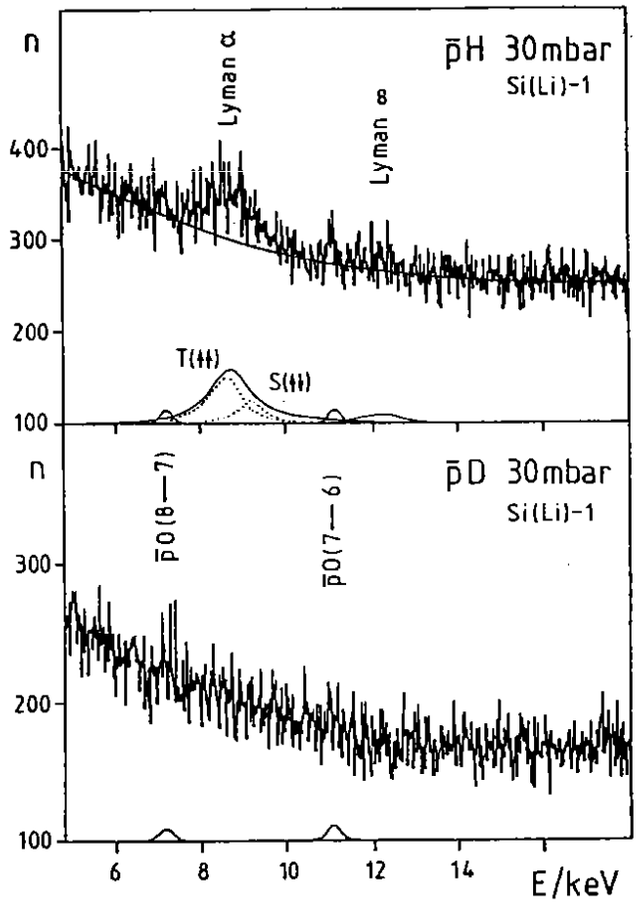

Fig. 8(c): Expanded view of the spectra shown in Fig. 8a for the energy region of the Ktransitions. The solid lines show the fit to the spin averaged Kα line in antiprotonic hydrogen, the dotted curves are from a fit to the triplet/singlet splitting (details see text). The antiprotonic oxygen transitions observed stem from a 10^{-2} mbar water vapor contamination in the target chamber. No structures are found in the deuterium spectrum which could be attributed to the Lyman transitions.

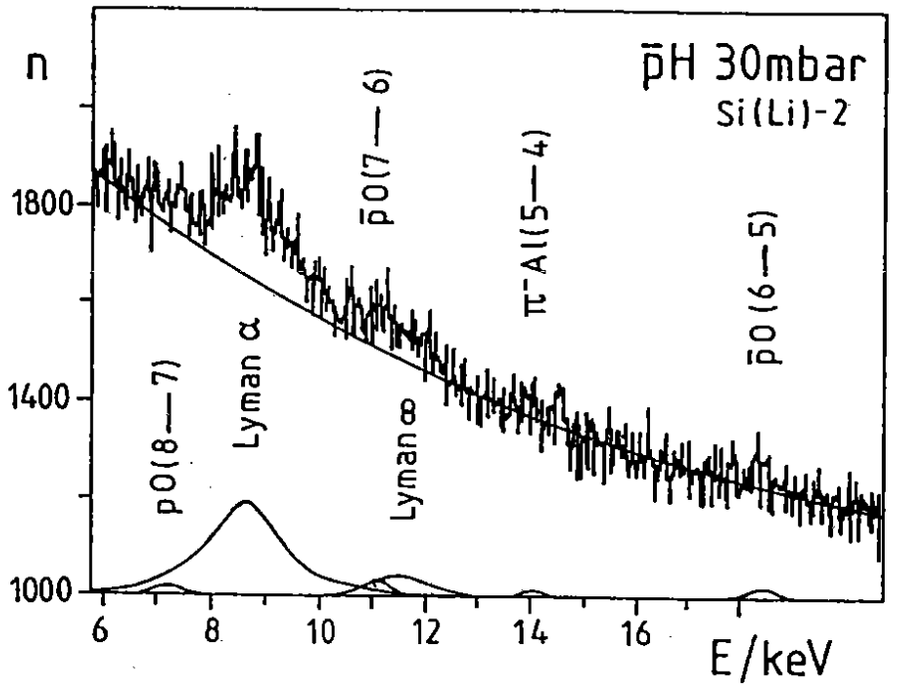

Fig. 9: X-ray spectrum measured with detector Si(Li)-2. The X-rays of pionic aluminum can be attributed to pions from stopped in the aluminum walls of the vacuum chamber.

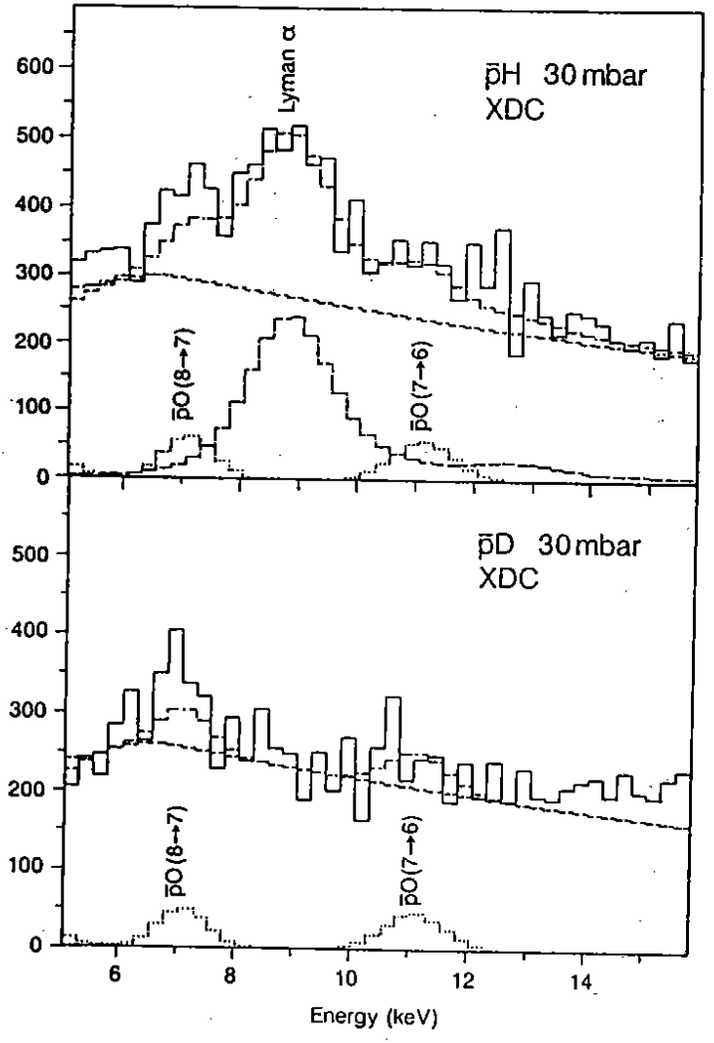

Fig. 10: X-ray spectrum for antiprotonic hydrogen (a) and deuterium (b) measured with the drift chamber. The solid line shows the filtered spectra (see text), the dashed-dotted line the background subtracted, and dashed line the resulting Lyman transition (for p̄H). Also shown with a dotted line are the two p̄O lines included in the background subtraction.

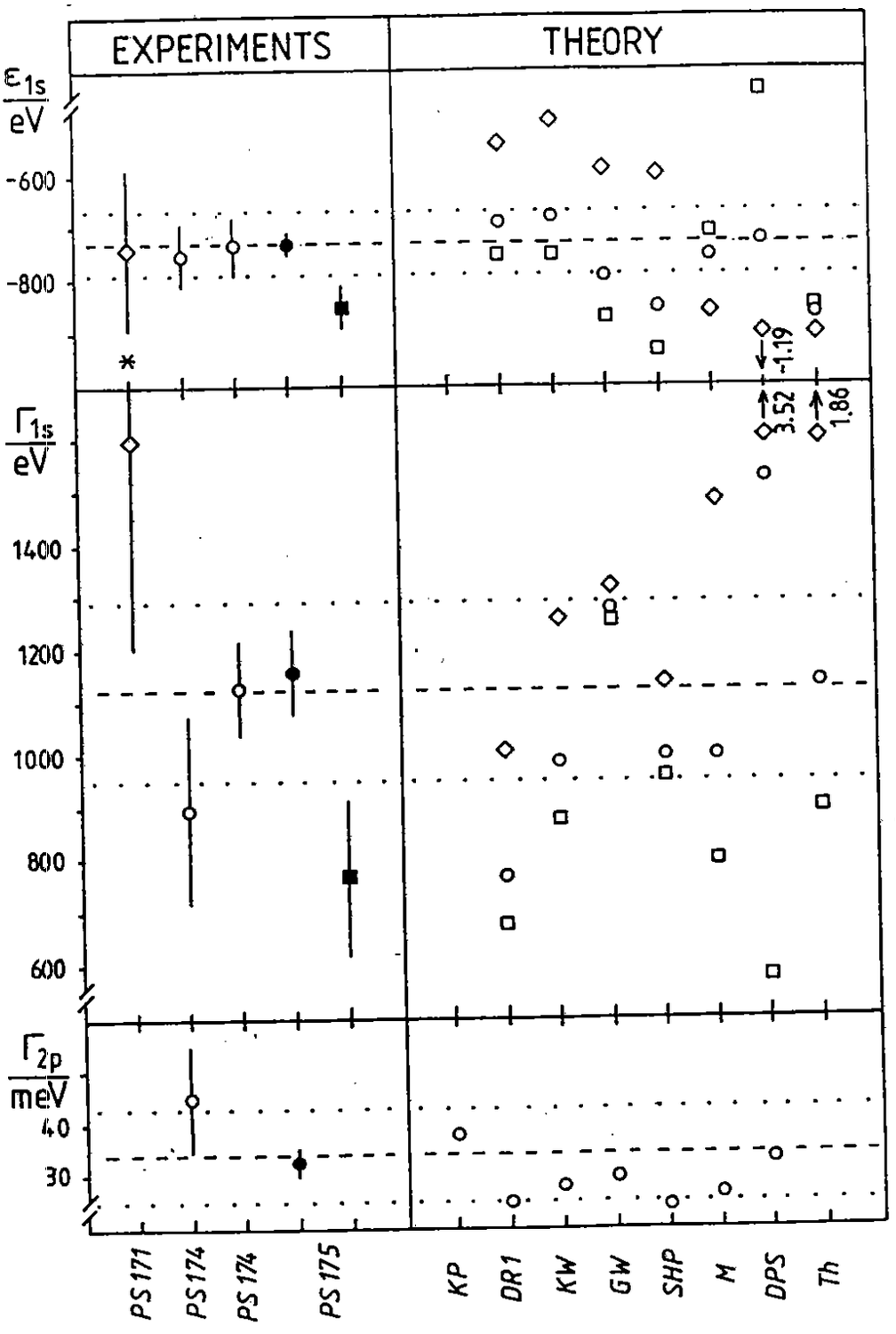

Fig. 11: Experimental results (1σ errors) of strong interaction shifts and widths (PS171 [27], PS174 [16,17], PS175 (see Table 3) with theoretical predictions (KP [28], DR1 [29], KW [29,30], GW[31], SHP [32], M [33], DPS [34] and Th [35]). The spin-averaged values of the theoretical models have been calculated taking into account the different absorption from the 2p hyperfine states (see text). The weighted averages of the experimental results are shown by dashed (mean value) and dotted (3σ errors) lines.

o o : spin averaged shift or width
◊ : singlet ground state $^1S_0$ of protonium
[] [] : triplet ground state $^3S_1$ of protonium
* : the shift is changed by - 40 eV to use the same value for the pure electromagnetic binding energy

(Full symbols: data from the present experiment).

Imprimé au CERN. Prix: 0.55 Fr.